Chemical Functionalization Effects on Armchair Graphene Nanoribbon Transport

ARTICLE *in* NANO LETTERS · JULY 2009

Impact Factor: 13.59 · DOI: 10.1021/nl900561x · Source: PubMed

Chemical Functionalization Effects on Armchair Graphene Nanoribbons Transport

Alejandro López-Bezanilla[1], François Triozon[2], Stephan Roche[3,4]
[1] *CEA, INAC/SPSMS/GT, 17 rue des Martyrs, 38054 Grenoble Cedex 9, France*
[2] *CEA, LETI-Minatec, 17 rue des Martyrs, 38054 Grenoble Cedex 9, France*
[3] *CEA, INAC/SP2M/L_sim, 17 rue des Martyrs, 38054 Grenoble Cedex 9, France*
[4] *Institute for Materials Science, TU Dresden, D-01062 Dresden, Germany*

(Dated: April 15, 2009)

We report first-principles transport calculations in chemically functionalized graphene nanoribbons. The effect of the joint attachment of hydroxyl and hydrogen groups on the graphene surface is investigated as a function of defect location and coverage density. The chemical bonding of a single defect pair (C-OH and C-H) is shown to considerably alter the conduction capability of short ribbon channels, similarly to a sp^3-type of defect. By performing transport calculations in disordered ribbons with lengths up to the micron scale, the elastic mean free paths and conduction regimes are analyzed. Even in the low grafting density limit, transport properties are found to be severely damaged by the functionalization, indicating a strong tendency towards an insulating regime.

PACS numbers:

The fabrication of a single graphene layer, either through exfoliation of graphite [1], or using epitaxial growth [2], has raised a huge amount of activities given the possibility to explore low dimensional transport in a material with spectacular electronic properties [3, 4], and owing to the perspective for carbon-based nanoelectronics [2, 5]. Reported charge mobilities in graphene layers can be as large as $\sim 2\ \mathrm{m^2V^{-1}s^{-1}}$ close to the Dirac point [6, 7]. Notwithstanding, as a peculiar two-dimensional system, a single graphene layer behaves as a zero gap semiconductor, with poor field effect capability. As a matter of fact, the charge current modulations (tuned by electrostatic gating) in undoped graphene layers hardly change by more than one order of magnitude [6]. To enable its use for designing active electronic devices, two strategies are proposed.

The first is based on the fabrication of graphene strips with reduced lateral size (known as graphene nanoribbons (GNRs)[8]) and larger energy bandgap. GNRs with width from several tens of nanometers down to 2 nm have been fabricated either by plasma etching [9] or by means of chemical treatment of graphite [10]. Band-gap engineering of GNRs has been demonstrated [11], and GNRs-based field effect transistors with good performances have been reported [12]. Alternatively, chemical functionalization of graphene-based materials is a promising strategy to reversibly tune 2D graphene electronic properties such as channel resistivity in field effect devices, without requiring aggressive ribbon width downsizing. For instance, a strong increase of the resistance of nitrophenyl functionalized graphene sheet has been recently reported [13]. Similarly, the design of reversible electrochemical switches based on chemically modified graphene, together with the fabrication of nonvolatile memory applications have been reported [14]. In this latter experiment, the water molecule from the ambient or at the SiO_2/graphene interface splits into H and OH groups, which are further assumed to attach to the graphene surface and open a large band gap. This effect was proposed to explain the measured modification of the channel resistivity by over six orders of magnitude [14].

Covalent functionalization of graphene materials triggers the formation of saturated sp^3 bonds which break the p_z network symmetry [15–19]. Obviously, this should induce a severe disruption of the otherwise good conducting properties of clean graphene, even yielding the possibility to grow graphene oxide, in case of massive coverage [20].

Additionally, beyond a reversible control of the current intensity, the possibility to induce chemical doping would enable the fabrication of either p-doped or n-doped graphene-based transistors, as shown for carbon nanotubes [21]. The recent experimental work by Farmer and coworkers [22] suggests that covalent chemical functionalization can induce significant doping of graphene-based devices. Finally, functionalization also allows the development of new applications such as chemical sensors [23, 24]. In this context, the understanding of the impact of covalent functionalization on charge transport in graphene-based material stands as a challenging issue.

In this Letter, we report a full *ab initio* study of the effect of chemical functionalization on charge transport in armchair GNRs. The joint attachment of hydroxyl and hydrogen groups onto the graphene surface is found to induce strong backscattering effects, with conductance patterns that are dependent on the functionalization sites. The results are shown to be related with the sp^3 nature of the chemical bonding. For armchair GNRs with initial large energy gaps, a superimposed functionalization-induced transport gap develops close to the band edges

and, at a fixed coverage density, widens with decreasing ribbon width or increasing ribbon length.

In the following we will refer to an armchair GNR composed of P dimer lines as *aPGNR* [26]. Armchair ribbons are all semiconductors but with different types of energy bandgaps. The two first studied ribbons (a17GNR and a35GNR) belong to the GNRs class with small energy bandgaps [26, 27]. Their widths range between 2.3 and 4.2 nm, which is within the reach of experiments [10]. Another type of GNRs (a16GNR and a34GNR) with much larger energy bandgaps will be also investigated [26, 27].

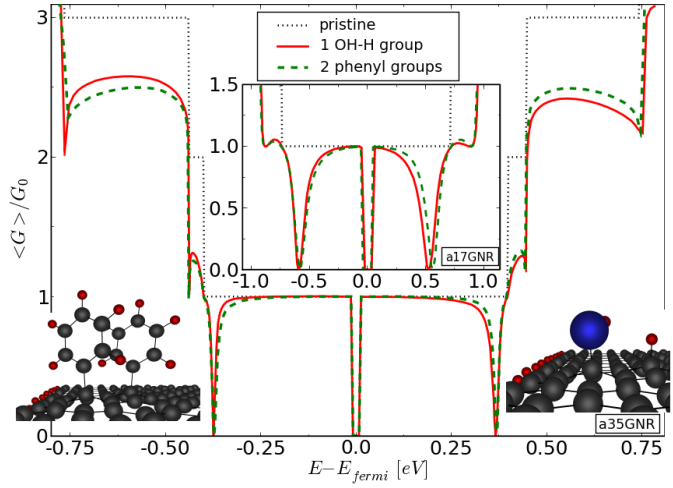

FIG. 1: (color online) Conductance of the a35GNR (main frame) and the a17GNR (inset) for the pristine case (doted lines) and for the single pair defect (C-OH, C-H) case (solid line). The case for a pair of phenyl groups is also given for comparison (dashed lines).

Our first principles calculations are performed using localized atomic-like basis set in the local density approximation (LDA) (SIESTA code [28, 29]), with a double-ζ basis for each atom. Spin polarized calculations within LSDA were also performed to check the multiplicity of the ground state. The triplet state ($S = 1$) is found to be 240 meV above the singlet state ($S = 0$), meaning that the presence of structural defects do not introduce higher multiplicity . In each case, the whole structure has been relaxed until residual forces were smaller than 0.04 eV/Å[30]. It is always observed that the length of the C-C bond near the edges is slightly shortened with regard to the central region of the ribbon. Indeed, after molecular dynamics relaxation, one observes that the anchorage C-atom sites are pulled a bit out (~ 0.7 Å) of the graphene plane, which in turn alters the coupling between such C atoms and their three neighboring C atoms, yielding a sp^3 defect conformation. Finally, one also notes that the bond length between a hydroxyl group and the anchorage C-atom site in the substrate is always larger when compared to the H counterpart bond, in agreement with prior energetics studies [20, 25]. Functionalization of graphene substrate with hydrogen adatoms has been recently reported using advanced transmission electron microscopy [31].

To compute the conductance of clean and defected GNRs, a multichannel Landauer-Büttiker technique as described in [32–34] is extensively used. The channel is defined between two perfect GNR-based right (left) leads (see Fig.3) which impose chemical potentials μ_1 (μ_2) and minimize the contact effects. The transmission coefficient $T(\epsilon)$ is obtained by solving the quantum mechanical problem of a single electron scattered within the channel. At zero temperature and in the low bias limit ($\mu_1 - \mu_2 = eV \rightarrow 0$), the conductance is given by $G = G_0 T(\epsilon)$, where $G_0 = 2e^2/h$ is the conductance quantum while ϵ denotes the energy of the incident charge carrier. Experimentally, the energy dependence of the conductance can be modulated through a capacitive coupling between the ribbon channel and a gate electrode. The transmission is calculated by evaluating retarded and advanced Green's functions of the system

$$\mathcal{G}^{\pm}(\epsilon) = \{\epsilon I - H - \Sigma_L^{\pm}(\epsilon) - \Sigma_R^{\pm}(\epsilon)\}^{-1} \qquad (1)$$

where $\Sigma^{\pm}_{L(R)}(\epsilon)$ are the self energies describing the coupling of the channel to the left and right leads. These quantities are related to the transmission factor by the Fisher and Lee relationship [35]

$$T(\epsilon) = tr\{\Gamma_L(\epsilon)\mathcal{G}^{+}(\epsilon)\Gamma_R(\epsilon)\mathcal{G}^{-}(\epsilon)\} \qquad (2)$$

with $\Gamma_{L(R)}(\epsilon) = i\{\Sigma^{+}_{L(R)}(\epsilon) - \Sigma^{-}_{L(R)}(\epsilon)\}$, whereas tr denotes the trace of the corresponding operator.

The computational approach is based on a technical strategy that is now well documented [33, 34, 36, 38]. At first, a large set of *ab initio* calculations are performed to obtain the Hamiltonian and overlap matrices associated with functionalized nanoribbon sections. Then, the complete disordered system is built up by randomly assembling such elementary parts containing a single or a few defects together with sections of pristine (clean) nanoribbons. This allows us to study transport through very long GNRs by using standard decimation techniques for the calculation of Green's functions and transmission probabilities [39].

For pristine ribbons, the electronic conductance is quantized $G = N_{\perp} G_0$, where $N_{\perp}$ is the number of active transverse modes available at the considered energy. Close to charge neutrality point, a single degenerated band is found in the first conductance plateau ($N_{\perp} = 1$).

Following prior studies for phenyl pairs [41] and OH/H functional groups [20], the grafted pair is such that the corresponding anchoring C-atoms are third nearest neighbors. This leads to the absence of local magnetic moments and broken bonds, which involves a gain of energy. Fig.1 (inset) and Fig.2 show the effect of a single pair of hydroxyl (OH) and hydrogen (H) groups (at different positions along the nanoribbon width) on the conductance of the a17GNR. The main effect of the defect is to induce zero conductance dips at two energies above and below the charge neutrality point. This is a clear signature of the sp^3 nature of the bonding as evidenced by

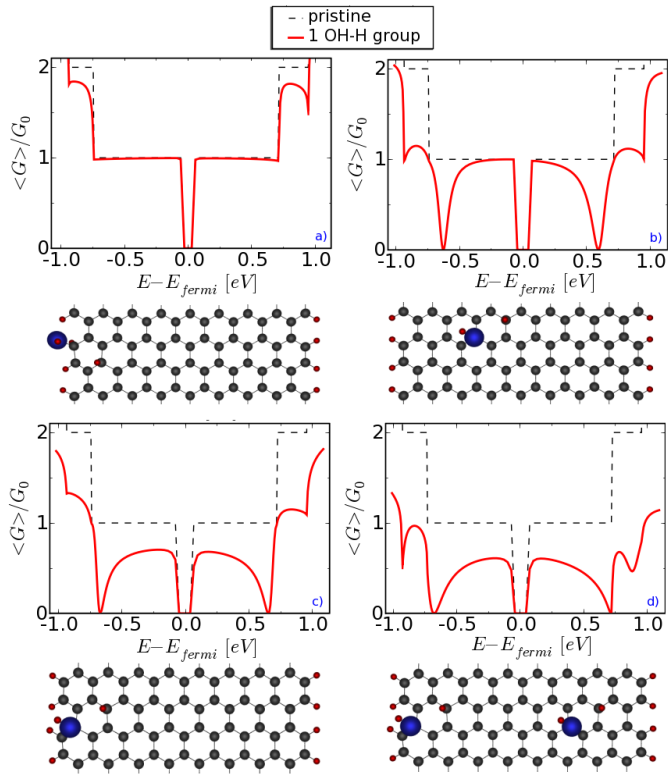

FIG. 2: (color online) Conductance of a17GNR as a function of defect position. The locations of the defects for a), b), c) and d) are illustrated at bottom. Case d) shows the conductance in case of two defects.

the comparison with the effect of a single phenyl pair on the same positions (see Fig.1 dashed lines). Note that a small electron-hole transport asymmetry is observed for the case of hydroxyl-hydrogen pair. This is likely to result from the asymmetric charge distribution around the new bonds between the grafted groups and the GNR substrate, while for the case of two phenyl groups no such asymmetry is observed, as both bonds are equivalent. The fact that our calculations for a grafted phenyl pair show no direct doping to the graphene material, supports the interpretation of [22] for a contact-induced doping effect driven by the functionalization. For higher energy subbands, the impact of a single defect is enhanced due to the increase of backscattering probability, as also found for less realistic disorder potentials [42]. One also notes that the influence of the asymmetry on backscattering is slightly more pronounced at higher energies.

The dependence of the a17GNR conductance as a function of the defect position is illustrated in Fig.2 for a set of typical configurations. If the C-OH bond is located at the GNR edge, a full suppression of backscattering is obtained in the first plateau (Fig.2-a), although some weak backscattering is seen for higher energy subbands. As discussed in [43] for NH_2, edge functionalization does not alter the electronic properties of the aGNR in the first subband since the impurity states are located far away from the Fermi level. In contrast, when the C-OH bond is shifted out of the edge line, the conductance is typically disturbed as shown in Fig.2-b or in Fig.2-c. Fig.2-b (see also Fig.1) shows similarity with the situation for pair of grafted phenyls, whereas other locations (Fig.2-c) exhibit a larger suppression of conductance in the first plateau, although higher energy subbands remain similarly affected. Such peculiar behavior of conductance depending on the OH/H pair location stems from the variation of screening effects that profile the precise scattering potential.

Fig.3 shows how the conductance is suppressed as the number of defects is increased along the width of a ribbon channel. The conductance decay is driven by both backscattering on individual functional groups together with quantum interferences that occur due to the proximity of the defects. The conductance of the short ribbon channel is fully suppressed up to high energies when a line of OH/H pairs is grafted along the width (not shown here). In the case of the ribbon channel shown in Fig.3,

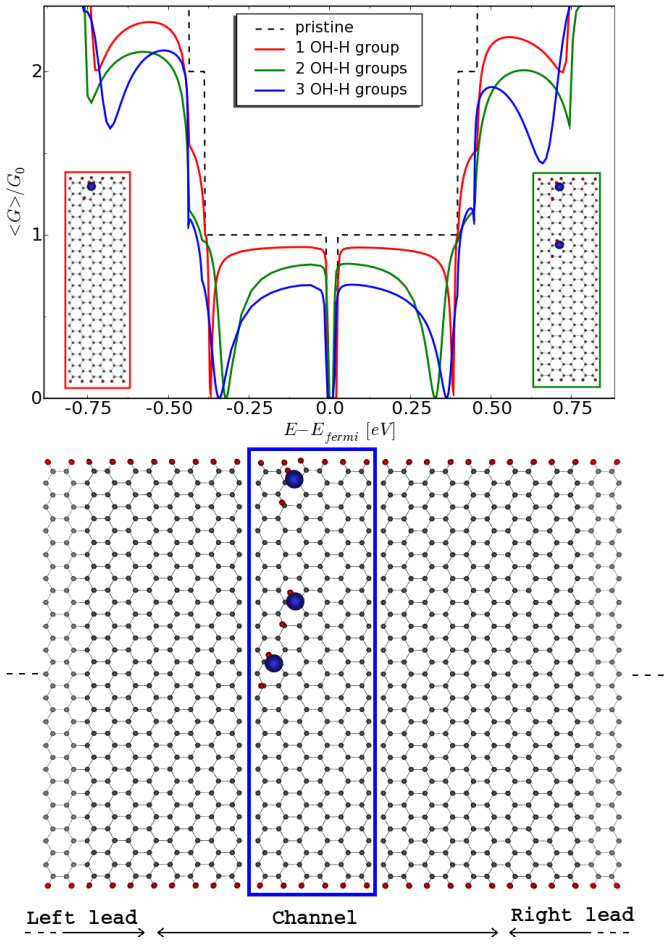

FIG. 3: (color online) Upper panel: Conductance of a35GNR with 1, 2 or 3 defects in a short ribbon channel (from top curve to bottom curve). Lower panel: Representation of the graphene-based structure used for the conductance calculation.

this corresponds to 9 OH/H pairs.

We further explore the conduction regime in long and disordered chemically functionalized aGNRs by computing configuration averaged conductance for aGNRs with varying defect density, length and width. As randomness is introduced in the defect distribution, both backscattering and quantum interferences are strongly enhanced, which ultimately leads to strong localization of states and full suppression of conductance.

The results obtained for the small-gaps a17GNR and a35GNR (Fig.4 left panel) are here compared with the other type of semiconducting GNRs (a16GNR and a34GNR) which display initially larger energy bandgaps (Fig.4 right panel). Fig.4 (left) shows how the averaged conductances of a17GNR and a35GNR decay when doubling the defect density (from 25 to 50 groups for a 200 nm long ribbon), or when increasing the length at a fixed density (from 200 to 600 nm). One notices a larger robustness of the conductance in the first plateau when compared with higher energy subbands, similarly to the single defect case (Fig.1, Fig.2 and Fig.3), but more pronounced for long disordered systems. This feature has been already observed for model disorder [42], and stems from the linear dispersion of excitations and pseudospin symmetry. This is clearly not the case for semiconducting armchair graphene ribbons a16GNR and a34GNR. As illustrated in Fig.4 (right-panel), the difference of the quantum transmission observed for a single OH-H defect between the a34GNR and the a35GNR, further develops as the number of attached molecules is increased. This results in a superimposed transport gap that widens the initial electronic bandgap. This phenomenon has been already discussed for edge defects [44–46] and is related to the enhanced contribution of quantum interferences that yield localization of states and insulating regime. This transport gap widens as the ribbon is further narrowed (for a fixed number of grafted groups) as shown in Fig.4 (right panel-inset).

To further contrast transport properties of different ribbons, the conductance scaling behavior is analyzed in Fig.5 at a fixed energy (marked with arrows in Fig.4). By using the formula $\langle G\rangle/G_0 = N_\perp(1+\frac{L}{l_e})^{-1}$ (where $\langle G\rangle$ denotes the average over 200 random defect configurations), one can infer the corresponding elastic mean free path (ℓ_e) that drives the scaling behavior. For the a35GNR, ℓ_e downscales from ~ 1 μm to ~ 200 nm, as the number of attached groups varies from 25 to 100. Since $\ell_e \geq L$ (L the channel length = 200 nm), the conduction mechanism is consistent with a quasiballistic regime. Similar behavior is found for the a34GNR for which ℓ_e decays from 850 nm to 260 nm for the same change in defect density. In contrast, for the a17GNR (resp. the a16GNR), ℓ_e decreases from 275 nm to 35 nm (resp. 20 to 10 nm), such that $\ell_e \ll L$, outlining that the electronic states are strongly localized along the ribbon channel. This is further confirmed by an exponential decay of the conductance versus ribbon length (not shown here).

In conclusion, by using a fully ab initio approach, we have analyzed the sensitivity of charge transport with respect to OH-H and phenyl pair defects attached to a graphene nanoribbon surface. The sp^3 nature of bonding of these defects onto graphene gives rise to strongly energy-dependent backscattering phenomena. Our results show a rapid decay of the conduction ability of armchair GNRs with increasing defect density and when reducing transport dimensionality. The opening of transport gaps has also been shown for the ribbon case which initially gives large energy bandgap. Further work is needed to account for the possible presence of intrinsic defects on the GNRs such as vacancies, edge defects, etc. Such defects with high chemical reactivity would also impact on the hydrogenation and functionalization processes (as discussed in [17–20]) with obvious consequences on the transport mechanisms.

The authors acknowledge Alain Rochefort for fruitful comments and the CEA/CCRT for providing computational resources. Financial support from the ANR/PNANO project ACCENT and EU/ICT GRAND projects are acknowledged. A.L.B is grateful to the Marie-Curie fellowship CHEMTRONICS programme. S.R. is indebted to the Alexander Von Humboldt Foundation for supporting his stay in TU-Dresden.

[1] Geim, A.K.; Novoselov, K.S. *Nature Materials* **2007**, 6, 183.
[2] Berger, C.; Song, Z.; Li, X.; Wu, X.; Brown, N.; Naud, C.; Mayou, D.; Li, T.; Hass, J.; Marchenkov, A.; Conrad, E.; First, P.; de Heer, W. *Science* **2006**, 312, 1191.
[3] Charlier, J.C.; Blase, X.; Roche, S. *Rev. Mod. Phys.* **2007**, 79, 677.
[4] Cresti, A.; Nemec, N.; Biel, B.; Niebler, G.; Triozon, F.; Cuniberti, G.; Roche, S. *Nano Research* **2008**, 1, 361.
[5] Wu, Y. Q.; Ye, P. D.; Capano, M. A.; Xuan, Y.; Sui, Y.; Qi, M.; Cooper, J. A.; Shen, T.; Pandey, D.; Prakash, G.; Reifenberger, R. *Appl. Phys. Lett.* **2008**, 92, 092192.
[6] Novoselov, K. S.; Geim, A. K.; Morozov, S. V.; Jiang, D.; Zhang, Y.; Dubonos, S. V.; Grigorieva, I. V.; Firsov, A. A. *Science* **2004**, 306, 666.
[7] Morozov, S. V.; Novoselov, K. S.; Katsnelson, M. I.; Schedin, F.; Elias, D. C.; Jaszczak, J. A.; Geim, A. K. *Phys. Rev. Lett.* **2008**, 100, 016602.
[8] Wakabayashi, K.; Fujita, M.; Ajiki, H.; Sigrist, M. *Phys. Rev. B* **1999**, 59, 8271
[9] Lemme, M.C.; Echtermeyer, T. J.; Baus, M.; and Kurz, H. *IEEE Electron Device Letters* **2007**, 28, 282.
[10] Li, X.; Wang, X.; Zhang, Li; Lee, S; Dai, H. *Science* **2008**, 319, 1229.
[11] Han, M. Y.; Özyilmaz, B.; Zhang, Y.; Kim, Ph. *Phys. Rev. Lett.* **2007**, 98, 206805.

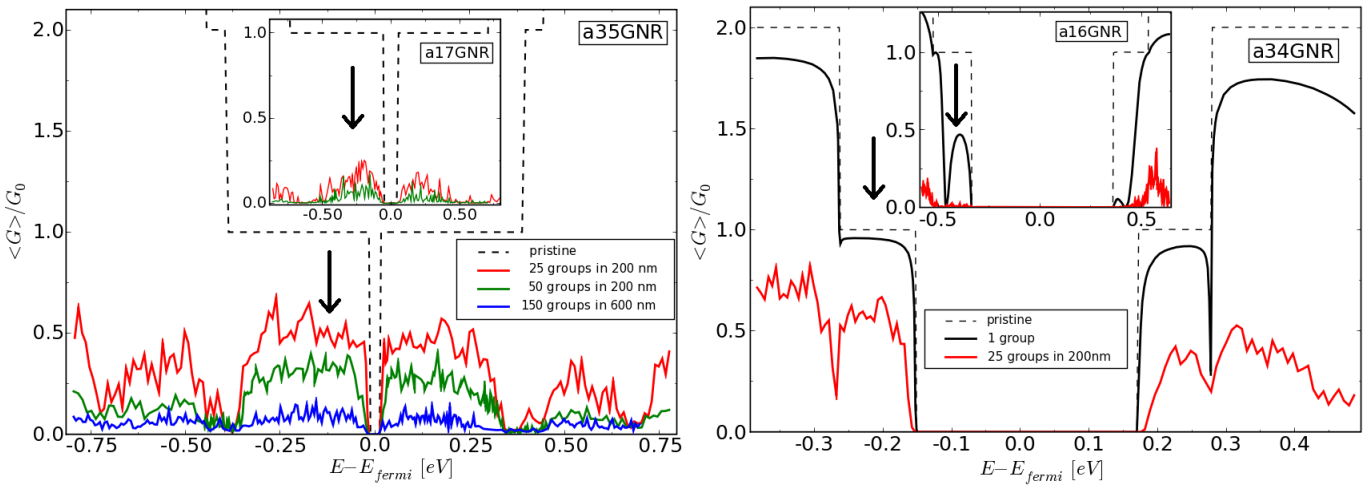

FIG. 4: (color online) Left Panel: Averaged conductance of the a35GNR and the a17GNR (inset) (in G_0 units) for different numbers of grafted groups and ribbon lengths. Right Panel: Same information for a34GNR and a16GNR (inset). Dashed lines give the conductance for the pristine cases.

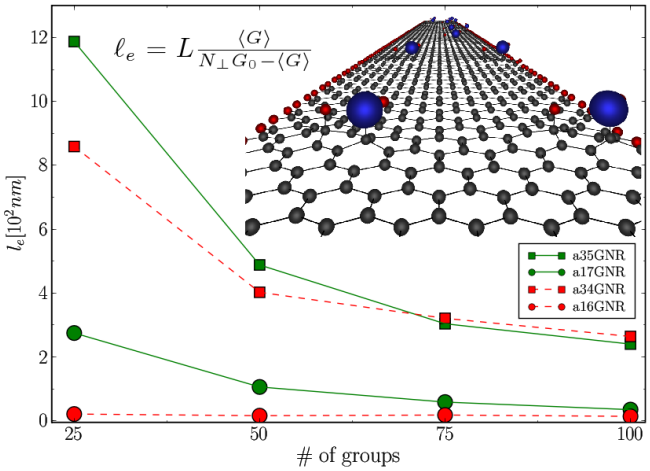

FIG. 5: (color online) Elastic mean free path as a function of number of attached pair OH-H defects for various graphene nanoribbons. The inset shows a picture of a given disorder configuration. The ribbon channel length is here $L = 200$ nm

[12] Wang, X.; Ouyang, Y.; Li, X.; Wang, H.; Guo, J.; Dai, H. *Phys. Rev. Lett.* **2008**, 100, 206803.

[13] Bekyarova, E.; Itkis, M.E.; Ramesh, P.; Berger, C.; Sprinkle, M.; de Heer, W.; Haddon, R.C. *J. Am. Chem. Soc.* **2009**, 131, 1336.

[14] Echtermeyer, T.J.; Lemme, M.C.; Braus, M.; Szafranek, B.N.; Geim, A.K.; Kurz, H. *IEEE Electron Device Letters* **2008**, 29, 952.

[15] Zhao, J.; Park, H.; Han, J.; Lu, J. *J. Phys. Chem. B* **2004**, 108, 4227.

[16] Boukhvalov, D.W.; Katsnelson, M. I. *J. Phys. Cond. Matt. to be published*, arXiv:0809.5257.

[17] Boukhvalov, D.W.; Katsnelson, M. I. *Nano Lett.* **2008**, 8 (12), 4373.

[18] Barone V.; Hod, O.; Scuseria G.E. *Nano Lett.* **2006**, 6, 2748.

[19] Hod O.; Barone V.; Peralta J.E.; Scuseria G.E. *Nano Lett.* **2007**, 7, 2295.

[20] Boukhvalov, D.W.; Katsnelson, M. I. *J. Am. Chem. Soc.* **2008**, 130, 10697.

[21] Derycke, V.; Martel, R.; Appenzeller, J.; Avouris, Ph. *Nano Lett.* **2001**, 1 (9), 453.

[22] Farmer, D. B.; Golizadeh-Mojarad, R.; Perebeinos, V.; Lin, Y.-M.; Tulevski, G.S; Tsang, J.C.; Avouris, Ph. *Nano Lett.* **2009**, 9, 388.

[23] Schedin, F.; Geim, A. K.; Morozov, S. V.; Hill, E. W.; Blake, P.; Katsnelson, M. I.; Novoselov, K. S. *Nature Materials* **2007**, 6, 652.

[24] Wehling,T. O.; Novoselov, K. S.; Morozov, S. V.; Vdovin, E. E.; Katsnelson, M. I.; Geim, A. K.; Lichtenstein, A. I. *Nano Lett.* **2008**, 8 (1), 173.

[25] Ito, A.; Nakamura, H.; Takayama, A. *J. Phys. Soc. Jpn.* **2008**, 77, 114602.

[26] Son, Y.-W.; Cohen, M.L.; Louie, S.G. *Phys. Rev. Lett.* **2006**, 97, 216803.

[27] White, C.T.; Li, J.; Gunlycke, D.; Mintmire, J.W. *Nano Lett.* **2007**, 7, 825.

[28] Ordejón, P.; Artacho, E.; Soler, J. M. *Phys. Rev. B* **1996**, 53, 10441.

[29] Artacho, E.; Sánchez-Portal, D.; Ordejón, P.; García, A.; Soler, J. M. *Phys; Stat; Sol. (b)* **1999**, 215, 809.

[30] To avoid any artificial backscattering effect in the coupling region, the supercell is chosen such that the influence of the grafting groups becomes negligible in the borders where periodic conditions are applied. To cope with this constraint we deal with large supercells containing up to 600 atoms. In all cases they are formed by 8 unit cells for armchair GNRs, with a total number of 560 C atoms for the a35GNR (544 C atoms for the a34GNR) and 272 C atoms for the a17GNR (256 C atoms for the a16GNR). The dangling σ bonds of edge C atoms are passivated by 32 H atoms following [26]. Each supercell contains from one to three OH and H grafted groups that have been placed at different positions along the ribbon width.

[31] Meyer, J.C; Girit, C.O; Crommie, M.F; Zettl, A. *Nature*

2008, 454, 319.
[32] Adessi, Ch.; Roche, S.; Blase, X. *Phys. Rev. B* **2006**, 73, 125414.
[33] Nardelli, M. B. *Phys. Rev. B* **1999**, 60, 7828.
[34] Triozon, F.; Lambin, Ph.; Roche, S. *Nanotechnology* **2005** 16, 230.
[35] Fisher, D. S.; Lee, P. A. *Phys. Rev. B* **1981**, 23, 6851.
[36] Biel, B.; García-Vidal, F. J.; Rubio, A.; Flores, F. *J. Phys.: Condens. Matter* **2008**, 20, 294214.
[37] Rocha, A. R.; Rossi, M.; Fazzio, A.; da Silva, A. J. R. *Phys. Rev. Lett.* **2008**, 100, 176803.
[38] Markussen, T.; Rurali, R.; Brandbyge, M.; Jauho, A. P. *Phys. Rev. B* **2006**, 74, 245313.
[39] López-Bezanilla, A.; Triozon, F.; Latil, S.; Blase, X., Roche, S. *Nano Lett.* **2009**, 9 (3), 940.
[40] Elias, DC; Nair, RR; Mohiuddin, TMG; Morozov, SV ; Blake, P; Halsall, MP; Ferrari, AC; Boukhvalov, DW; Katsnelson, MI; Geim, AK ; Novoselov, KS *Science* **2009**, 323, 610.
[41] Jiang, D.E.; Sumpter, B.G.; Dai, S. *J. Phys. Chem. B* **2006**, 110, 23628.
[42] Areshkin, D. A.; Gunlycke, D.; White, C. T. *Nano Lett.* **2007**, 7, 204.
[43] Cervantes-Sodi, F.; Csanyi, G.; Piscanec, S.; Ferrari, A. C. *Phys. Rev. B* **2008**, 77, 165427.
[44] Evaldsson M.; Zozoulenko, I.V.; Xu, H.; Heinzel, T. *Phys. Rev. B* **2008**, 78, 161407.
[45] Mucciolo, E. R.; Castro Neto, A.H.; Lewenkopf, C. H. *Phys. Rev. B* **2009**, 79, 075407.
[46] Naumis, G. *Phys. Rev. B* **2007**, 76, 153403.